Available online at www.sciencedirect.com
SCIENCE DIRECT®
Electrochemistry Communications 8 (2006) 173–178
electrochemistry communications
www.elsevier.com/locate/elecom

Local oxidation characteristics on titanium nitride film by electrochemical nanolithography with carbon nanotube tip

Te-Hua Fang *, Kuan-Te Wu

Institute of Mechanical and Electromechanical Engineering, National Formosa University, Huwei, Yunlin 632, Taiwan

Received 5 August 2005; received in revised form 22 October 2005; accepted 8 November 2005

Abstract

The oxidation characteristics of TiN thin films by atomic force microscopy (AFM) electrochemical nanolithography with multiwalled carbon nanotube tip was investigated. The TiN films were produced on silicon substrate by atomic layer chemical vapor deposition (ALCVD). The electrochemical parameters, such as anodized voltages, oxidation times, writing speeds, pulse voltage periods and how they affected the creation and growth of the oxide nanostructures were explored. The results showed that the height of the TiN oxide dots grew as a result of either the anodization time or the anodized voltage being increased. The oxide growth rate was dependent on the anodized voltage and on the resulting electric field strength. Furthermore, as the electric field strength was at an order of 2×10^7 V/cm, the anodization rate decreased quickly and the oxide dots stopped growing. Auger electron spectroscopy (AES) measurements confirm the modified structures took the form of anodized TiN.

Keywords: Atomic force microscopy; Carbon nanotube; Nanolithography; TiN; ALCVD

1. Introduction

During the past decade, scanning probe microscopy (SPM) such as scanning tunneling microscopy (STM) and atomic force microscopy (AFM) have had a great impact on the development of the nanotechnology because of their demonstrated ability to manipulate atoms on the surface and to fabricate nanostructures [1]. Scanning probe anodization is a nanolithographic technique based on the electrochemical oxidation of a specimen with an adsorbed water layer [2]. In particular, an AFM-based local anodization process has been investigated for the fabrication of nanostructures and nanodevices [3,4].

The multiwalled carbon nanotube (MWNT) has been suggested as the ultimate high-resolution probe for AFM because of its excellent properties, such as its high aspect ratio, small diameter, selective chemical reactivity, excellent mechanical robustness and electrical conductivity, which provide great advantages for imaging and writing tools compared to conventional silicon-based tips [5,6]. Conventional atomic force microscope tips attached with MWNT can offer many advantages in nanoscale imaging and lithography. Due to its geometric characteristics, structure, electronic and chemistry, the carbon nanotube has actually found to be quite useful in imaging surface structures at greater depths and softnesses as well as prolonging the life time of the probe's tip. Due to the high aspect ratio of the MWNT probe, it is able to produce better images of microcircuits being deeper and narrower than those produced by silicon probes. Cooper et al. [7] has achieved Terabit-per-square-inch data storage on titanium surfaces by AFM nanolithography with a CNT probe. Moreover, CNT has good mechanical properties in terms of high Young's modulus and good flexibility, which make it more suitable to be the AFM probe than other materials presently [8,9].

Atomic layer chemical vapor deposition (ALCVD) is a promising technique for growing semiconductor materials with excellent step coverage and excellent thickness uniformity by means of atomic level layer-by-layer deposition on

* Corresponding author. Tel.: +886 5631 5395; fax: +886 5631 5394.
E-mail address: fang.tehua@msa.hinet.net (T.-H. Fang).

1388-2481/$ - see front matter © 2005 Elsevier B.V. All rights reserved.
doi:10.1016/j.elecom.2005.11.005

a large-area wafer [10]. Titanium nitride (TiN) films have been employed for ultra large-scale integration (ULSI) because of its high thermal stability, low electrical resistivity and good diffusion barrier characteristics [11].

AFM-induced oxidation on TiN thin films produced TiO_xN_y oxide structures [12]. TiO_xN_y has excellent dielectric properties for microelectronics or high-density-storage applications. Also, TiN_xO_y films can be used for many other useful applications, such as solar selective absorbers, wear-resistant coatings and as a low-adhesive surface material, to reduce the formation of bacterial-biofilms on biomaterials. However, there is still a lack of information concerning the surface's anodic kinetics, growth mechanisms, and the effect of the electric field strength using AFM with a MWNT tip. In this study the MWNT probe tip-induced local anodization on TiN surface is presented.

2. Experimental details

The TiN thin films were deposited on a p-type Si(1 0 0) substrate by ALCVD. Before the film's deposition, the Si wafer was cleaned in a HF solution to remove the native oxide SiO_2 layer. $TiCl_4$ and NH_3 reaction gases were supplied sequentially during the deposition process [13]. Ar was used as a purge gas to remove the chemical residue with no adsorption to the surface. The amount of time each gas was sequentially supplied for $TiCl_4$, Ar purge, NH_3 and Ar purge was 5, 4, 1 and 5 s, respectively. The possible reaction for the ALCVD using precursors of $TiCl_4$ and NH_3 is as follows:

$$6TiCl_4 + 8NH_3 \rightarrow 6TiN + 24HCl + N_2 \quad (1)$$

A SPM was used in tapping mode to measure the surface morphology and surface roughness of the TiN films. The average surface roughness of the TiN films at the temperatures of 350, 400, 450 and 500 °C were approximately 1.7, 0.7, 0.6 and 0.4 nm, respectively. The typical thickness of the TiN films was about 10 nm. The film's resistivity was measured using the four-point probe method at room temperature. The resistivity of the TiN films at the temperatures of 350, 400, 450 and 500 °C were about 710, 325, 250 and 145 μΩ cm, respectively. As the deposition temperature was increased, the surface roughness and the resistivity of the TiN films decreased. In this study the TiN film with the best surface behavior was at the deposition temperature of 500 °C and it was chosen to explore its oxidation characteristics. The substrate temperature during the deposition process was kept at 500 °C and the pressure was at about 133 N m^{-2}.

The local oxidation experiments were performed using an AFM (NT-MDT Solver, Russia) with a carbon nanotube probe (Nanoscience Instruments, USA) as shown in Fig. 1. The carbon nanotube probe consisted the multi-wall nanotube tip that was mounted onto a commercial AFM etched silicon probe. The carbon nanotube diameter is about 30 nm. An Al reflective layer of 30 nm was coated on the AFM cantilever backside. The cantilever length and spring constant of the AFM probe were 125 μm and 40 N m^{-1}, respectively. In this technique, the oxide structures grew on the chemically reactive surfaces by the application of a bias voltage between the surface and the AFM probe tip. Composition of the oxide and the film was characterized by Auger electron spectroscopy (AES, VG Microlab 310D, USA) with incident electron energy of 10 keV. The AFM probe was used as the cathode and the adsorbed water created from an ambient humidity of 60% was used as the electrolyte in non-contact mode. The feedback system was turned off and the bias voltage was applied to perform the local oxidation experiment in the non-contact mode. The thickness of the water film at 60% humidity was more than 1 nm and less than 10 nm and the capillary force and the surface tension between the AFM tip and the water layer affected the continuity of the water layer. The pulse duration was set as 20 s. When the electric field was greater than 2×10^7 V/cm and the water meniscus adsorbed on the specimen surface provided the oxyanions oxide structures were formed on the surface.

3. Results and discussion

The mechanism of AFM local anodic oxidation of a TiN surface is depicted in the Fig. 1. The AFM local anodic oxidation mechanism of a TiN surface is depicted in the Fig. 1. There is an adsorbed water layer on the surface,

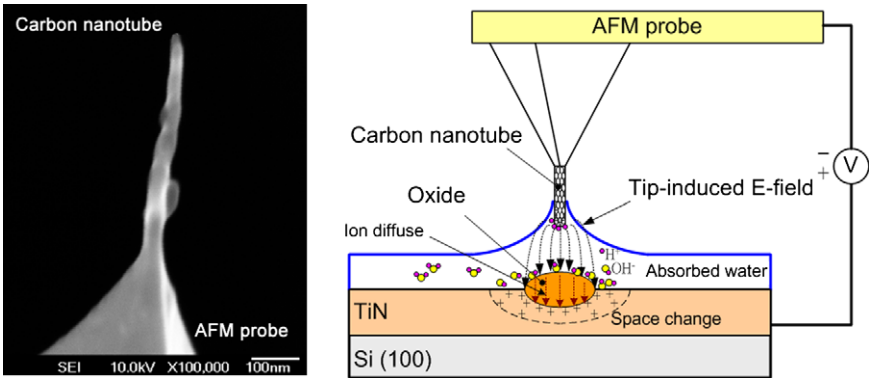

Fig. 1. Schematic of electrochemical principle of AFM with a carbon nanotube probe and SEM image of the carbon nanotube probe.

which provides the required electrolyte under ambient conditions. The thickness of the water layer depends on the amount of relative humidity introduced into the air in the sealed environment. Using the AFM tip as a cathode, the surface of the TiN film will become oxidized, and the ions (including OH^- and O^{2-}) contribute to the formation of the surface oxide which then produces the nanooxidized structure. The oxidation mechanism occurred on the surface of the TiN film as follows: When setting the AFM tip near the TiN surface, the Faraday current flowed from the tip through the water to the TiN surface. Then, the TiN surface became oxidized to form the oxidized tantalum oxynitride (TiN_xO_y) structure. By scanning the AFM tip, over the samples surface TiN_xO_y were formed. The formation of a TiN_xO_y compound could result from the replacement of nitrogen by oxygen or defects in the TiN surface could favor the incorporation of oxygen in the cation sublattice. The possible chemical reactions at the AFM tip/water interface and the TiN/water interface are described as follows:

AFM tip/water interface

$$4H^+ + 4e^- \rightarrow 2H_2 \quad (2)$$

TiN/water interface

$$x\mathrm{TiN} + yh^+ + yOH^- \rightarrow \mathrm{TiN}_x\mathrm{O}_y + yH^+ \quad (3)$$

where h^+ stands for a hole.

Figs. 2a and 2b represent the oxide height and oxide width at anodization voltages of 7–10 V and as a function of the anodization time. Fig. 2c depicts a sequence of AFM imaged oxide dots fabricated using the AFM-based oxidation method. The patterns in Fig. 2c were obtained by using the static voltages of 10 V at the different oxidation times of 0.5, 1, 2, 5 and 10 s. These experiments were carried out in an environment having a relative humidity of 60%. It can be seen that the oxide height and width increased as the logarithm of the anodization time increased and as the anodization voltage was increased. The observed relationship of the oxide nanodot height to the probe tip's oxidation time can be explained by the field-assisted oxidation theory of thin films [14]. The largest oxide nanodots corresponded to the longest oxidation time. The oxide dots had not only grown along the vertical direction but also along the horizontal direction. The lateral resolution was determined by the oxide nanodot's width and was found to be proportional to the oxide nanodot's height.

To fabricate a dot for a given size the anodization times should be shortened or lengthen in relationship to the corresponding anodization voltages which would be increased

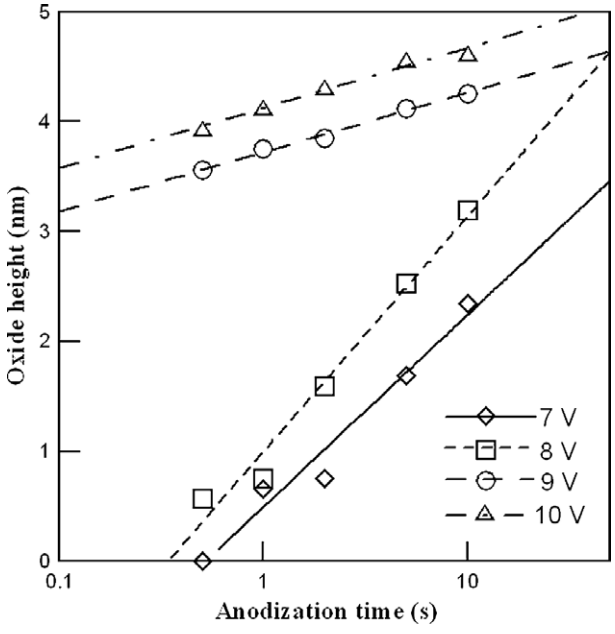

Fig. 2a. Oxide height of the oxidation process under different anodization times.

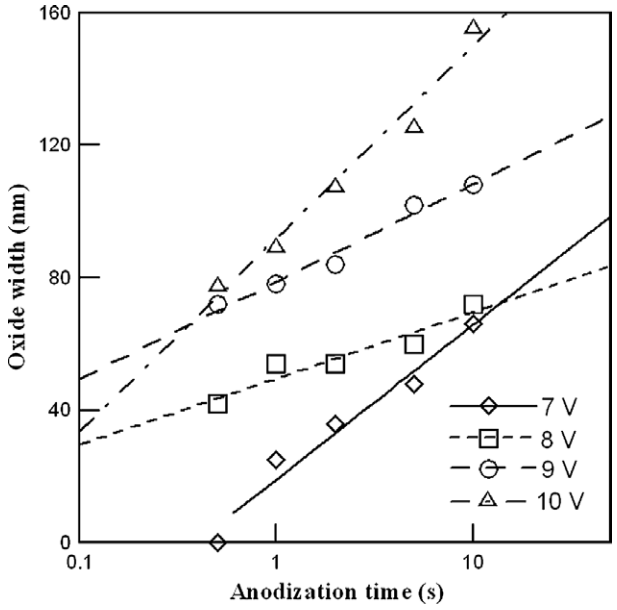

Fig. 2b. Oxide width of the oxidation process under different anodization times.

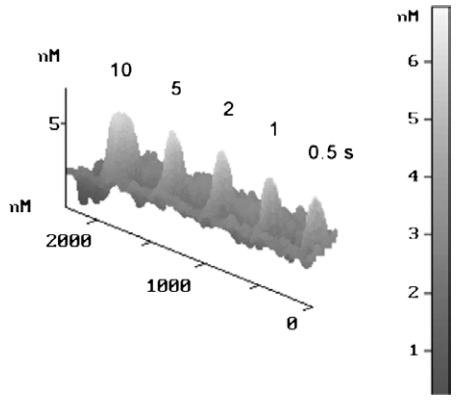

Fig. 2c. From right to left, an AFM image of five oxide dots fabricated on the TiN surface at the different anodization times of 0.5, 1, 2, 5 and 10 s, which were obtained at 10 V.

or decreased, respectively. This is to say when using a shorter anodization time a higher anodization voltage should be use and when using a longer anodization time a lower anodization voltage should be use to fabricate dots of equal mechanisms and proportion.

To understand the oxide growth rate, experiments were performed to determine the kinetics of the oxide process. The different size oxide dots were analyzed at the anodized voltages of 7–10 V and between the anodization times of 0.005–100 s. During the AFM tip-induced anodization process, the electric field enhanced the occurrence of the ion diffusion mechanism. The relationships of the growth rate and the electric field strength at a relative humidity of 60% are shown in Fig. 3a. In Fig. 3a it can be seen that the larger lateral growth rates were obtained and therefore a higher electric field strength occurs when the applied anodization voltages was larger. The initial lateral growth rate was on the order of ~100 nm/s at applied voltages of 9 and 10 V, and rapidly became smaller when the electric field strength was smaller. When the applied voltage increased, the initial lateral growth rate was increased. The anodization process was enhanced when the electric field strength was at an order of $\sim 2 \times 10^7$ V/cm.

As pointed out in Avouris et al. [14], an equation was used to describe the growth kinetics as follows:

$$\frac{dH}{dt} \propto \exp\left(-\frac{H}{l_c}\right) \tag{4}$$

where H is the oxide thickness at time t, and l_c is a characteristic length depending on the anodization voltage. The relationships between the lateral growth rate and the oxide height at four different applied bias voltages of 7, 8, 9 and 10 V are plotted in Fig. 3b. In this experiment it was observed that the larger the oxide height was the slower the lateral growth rate became. The applied bias voltage extended the electric field strength assisting the oxidation mechanisms until the growth was limited by the diffusion. The oxide rate is not only a function of electric field strength but also appears to depend on the bias voltage applied to the probe. The Cabrera–Mott theory [15] of field-induced oxidation cannot account for this kinetics observed in this experiment. Attempts to explain the differences between the kinetics of AFM-induced oxidation and the Cabrera–Mott field model have invoked the thought that the possible reasons are such mechanism as: the mechanical stress created and arisen within the oxide dots because of a large volume mismatch between the specimen and the oxide dot's structure [16]; the space charge build-up within the oxide dots [17]. The expected volume of the object increased as the oxidation reaction was increased. The expected volume expansion might be due to stress relief causing the formation of defect-rich oxide. The volume of the dot continued to increase until the maximum growth rate was reached and then it began to decrease.

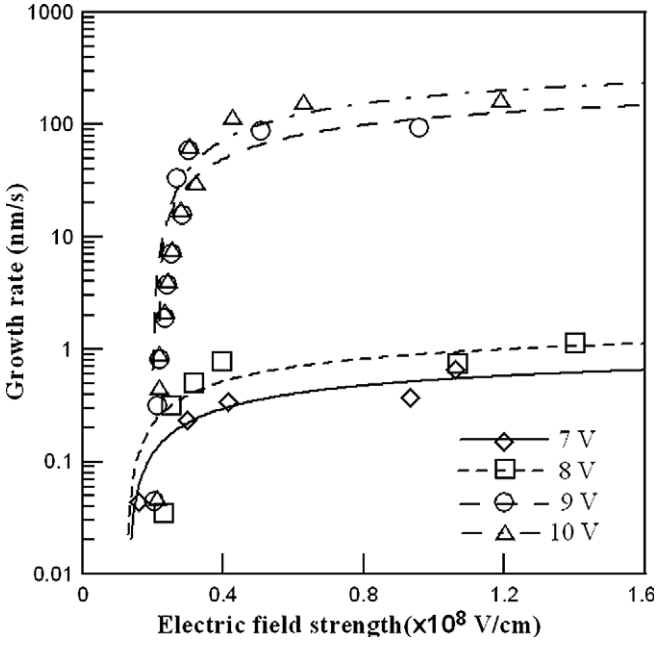

Fig. 3a. Growth rate vs. electric field strength.

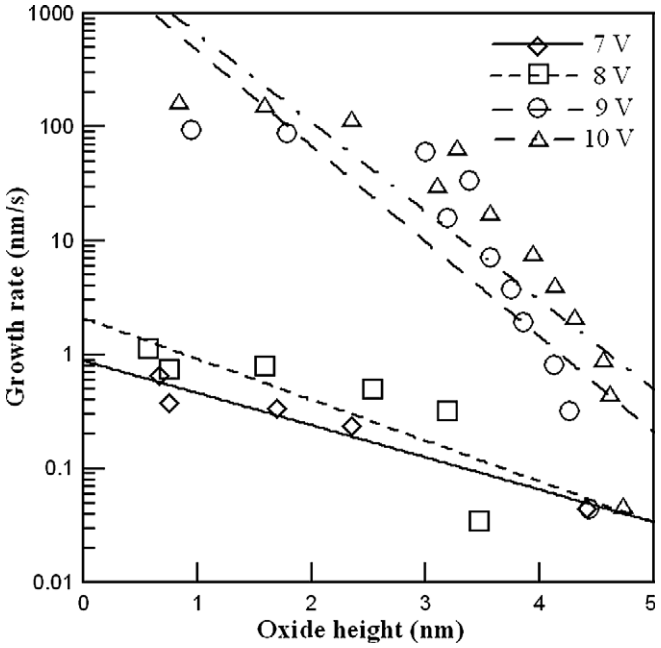

Fig. 3b. Growth rate vs. oxide height.

In order to explore the growth behavior of the oxide, dot patterns were fabricated by applying voltages with on/off pulse durations of 0.01–1 per second. The pulse voltage had a square wave with a constant amplitude and a rest amplitude of 0 V. The relative humidity was kept at 60% during the anodization process. Fig. 4 shows the dependence of the width of the oxide dots using different pulse periods under anodization voltages of 7–10 V. OH^- was generated from the water meniscus between the tip and the sample's surface. Once the voltage was applied to the MWNT tip, the OH^- ions drifted to the sample's surface due to the locally produced electric field. The ions arrived at the sample's surface at different time and the drifting

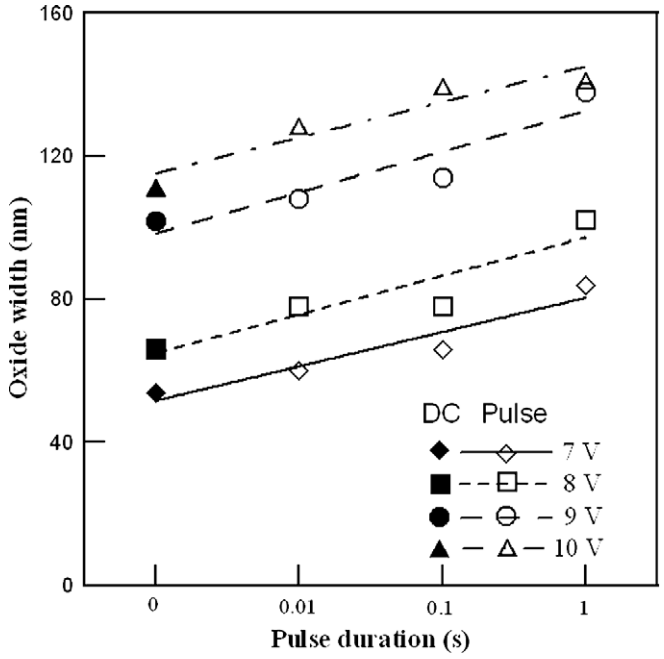

Fig. 4. Oxide width of the oxidation process under different period of pulse voltage.

speeds of the ions were spatially different contributing to the formation of the surface oxides. Under the tip the sample's surface was initially oxidized and then the oxidized region would spread out. The lateral growth rate of the oxide would decrease when the electric field strength decreased rapidly around the central oxidized region. It can be seen that a larger oxide structure was created by the pulse voltage period than that of the static DC voltage. This reason can be explained by the static DC voltage being applied to the AFM tip and OH^- ions drifting through the anode continuously inducing the growth of the oxide on the sample's surface. If a pulse voltage is applied, the transportation of OH^- ions will be broken during the rest duration of the pulse voltage and will cause the oxidation growth to stop. When the next pulse voltage is started, the transportation of the OH^- ions will reinitialize. This is due to the OH^- ions traveling randomly during the rest period of the pulse.

A moving MWNT tip was used to create the nanowires. This method can easily control the growth configuration and generation position of the TiN oxide nanowire. In order to understand how the tip speed affects the oxide nanowire the static DC voltage operation was used under different tip speeds. Fig. 5 shows the relationship of the tip speeds on the oxide height and width. The oxide nanowire was generated at the applied voltages of 7, 8, 9 and

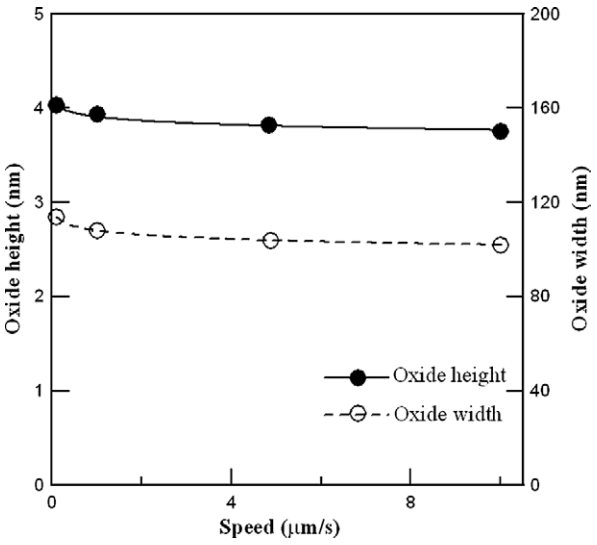

Fig. 5. Oxide height and width at different scanning speeds.

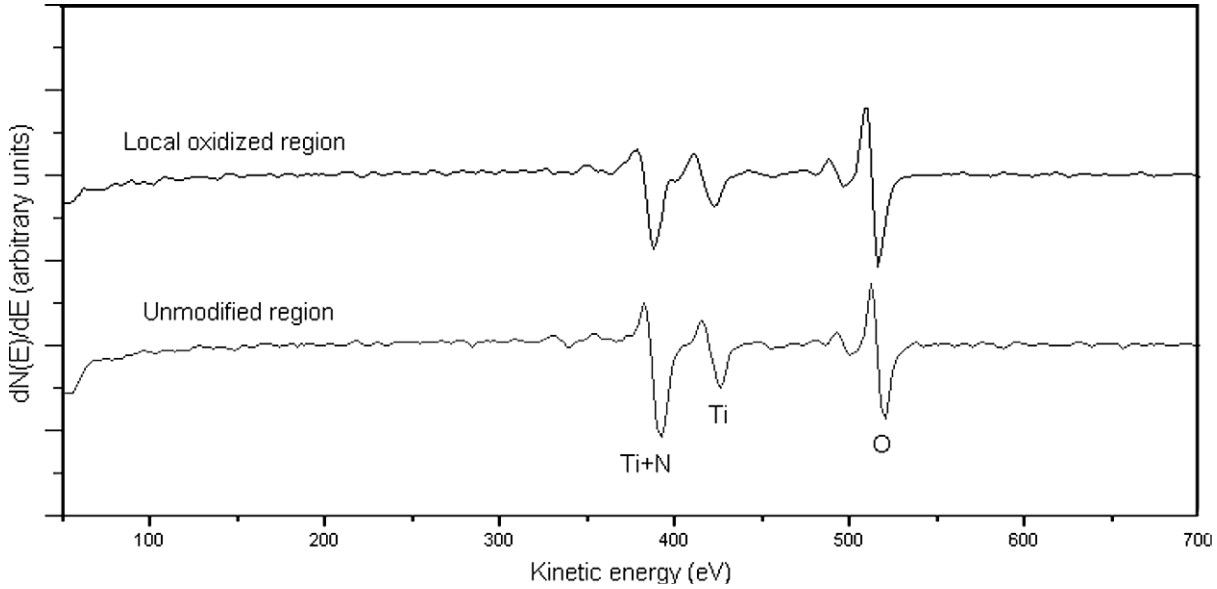

Fig. 6. Auger analysis on both local oxidized region and unmodified region of the TiN film.

10 V and at a relative humidity of 60%. When a higher speed was used to induce the oxide, a slightly lower height of the nanowire was achieved at tip speeds of 0.1–10 μm/s. Comparing the height of the nanowires between that of nanodots under the same voltage. The height of the nanodots was found to be higher than that of the nanowire. The scanning tip produces nanowires with smaller heights due to both a decreased oxidation time and a reduced residence time.

In order to understand the composition of the local oxidized structure, Auger electron microscopy analysis was conducted on an oxidized zone of $10 \times 10\ \mu m^2$. The Auger spectra of the local oxidized region and the unmodified region are shown in Fig. 6. It can find that the clear emission peak of O with kinetic energy of about 502 eV. The oxygen to Ti intensity ratio is greater in the local oxidized region than that in the unmodified region. This is consistent with the result of the previous study [18]. They suggested that an enhanced incorporated process of oxygen occurred and the weaker oxygen occurred in the unmodified region originated from the native oxide [18].

Chemical analysis of the TiN is complicated by the fact the $KL_{23}L_{23}$ Auger electron emission from nitrogen occurred at energy that overlaps the $L_3M_{23}M_{23}$ transition from Ti at the kinetic energy of about 385 eV [19]. The Auger electron microscopy results were similar to Gwo et al. [12] pervious study. Since there is no N Auger transitions kinetic energy above 400 eV, the $L_3M_{23}M_{45}$ transition of Ti occurs at the kinetic energy of about 418 eV [12]. This result showed that the anodic oxidized TiN films contains the TiN_xO_y transition layer.

4. Conclusion

In summary, the mechanism of TiN anodization process was investigated by applying an anodized voltage to the AFM MWNT tip. The TiN oxides were created by AFM oxidation nanolithography. The oxide thickness was found to increase as the anodized voltage or the anodized time was increased. The greater the oxide structures thickness became the weaker the electric field strength became, which also limited the oxide structures growth. The oxide thickness was governed by the electric field strength. The TiN-oxide nanostructures were successfully fabricated and the mechanisms studied during the anodization process. These results show that AFM nanooxidation with a MWNT tip is to be a promising method for fabricating TiN thin films and has great potential for use in the fabrication of future nanodevices applications.

Acknowledgement

This work was partially supported by National Science Council of Taiwan, under Grant No. NSC94-2212-E150-046.

References

[1] Y. Zhang, E. Balaur, S. Maupai, T. Djenizian, R. Boukherroub, P. Schmuki, Electrochem. Commun. 5 (2003) 337.
[2] S. Shingubara, Y. Murakami, K. Morimoto, T. Takahagi, Surf. Sci. 532–535 (2003) 317.
[3] M. Lazzarino, S. Heun, B. Ressel, K.C. Prince, P. Pingue, C. Ascoli, Appl. Phys. Lett. 81 (2002) 2842.
[4] S.R. Jian, T.H. Fang, D.S. Chuu, J. Phys. D 38 (2005) 2424.
[5] S.S. Wong, E. Joselevich, A.T. Wolley, C.L. Cheung, C.M. Lieber, Nature 394 (1998) 52.
[6] H. Dai, N. Franklin, J. Han, Appl. Phys. Lett. 73 (1998) 1508.
[7] E.B. Cooper, S.R. Manalis, H. Fang, H. Dai, K. Matsumoto, S.C. Minne, T. Hunt, C.F. Quate, Appl. Phys. Lett. 75 (1999) 3566.
[8] T.H. Fang, S.R. Jian, D.S. Chuu, Chinese Phys. Lett. 21 (2004) 1117.
[9] Y.R. Jeng, P.C. Cha, T.H. Fang, J. Phys. Chem. Solids 65 (2004) 1849.
[10] H. Zhang, R. Solanki, B. Roberds, G. Bai, I. Banerjee, J. Appl. Phys. 87 (2000) 1921.
[11] M. Wittmer, Appl. Phys. Lett. 36 (1980) 456.
[12] S. Gwo, C.L. Yeh, P.F. Chen, Y.C. Chou, T.J. Chen, T.S. Chao, S.F. Hu, T.Y. Huang, Appl. Phys. Lett. 74 (1999) 1090.
[13] T.H. Fang, Electrochim. Acta 50 (2005) 2793.
[14] P. Avouris, T. Hertel, R. Martel, Appl. Phys. Lett. 71 (1997) 285.
[15] N. Cabrera, N.F. Mott, Rep. Prog. Phys. 12 (1949) 163.
[16] Y. Okada, S. Amano, M. Kawabe, J.S. Harris Jr., J. Appl. Phys. 83 (1998) 7998.
[17] T.H. Fang, Microelectron. J. 35 (2004) 701.
[18] K. Matsumoto, S. Takahashi, M. Ishii, M. Hoshi, A. Kurokawa, S. Ichimura, A. Ando, Jpn. J. Appl. Phys. 1 34 (1995) 1387.
[19] P.T. Dawson, K.K. Tzatzov, Surf. Sci. 149 (1995) 105.